Progress In Electromagnetics Research B, Vol. 95, 41–60, 2022

Millimetric-Wave Quad-Band MIMO Antennas for Future Generations of Mobile Communications

May Abo. El-Hassan, Asmaa E. Farahat*, and Khalid F. A. Hussein

Abstract—Two types of quad-band millimetric-wave four-port MIMO antenna systems are proposed for the forthcoming generations of mobile handsets. A novel printed antenna is introduced to be the single-element of the MIMO antenna system. It is shown that the proposed MIMO antennas are capable to produce both spatial and polarization diversities that enhance the performance of mobile communications. A co-polarized four-port MIMO antenna is proposed to provide spatial diversity whereas another cross-polarized four-port MIMO antenna is proposed to produce both spatial and polarization diversities. It is shown that the two types of MIMO antennas can operate efficiently over the four frequency bands centered at 28, 43, 52, and 57 GHz. Prototypes are fabricated for the proposed MIMO antennas for the sake of experimental evaluation. Both the experimental and simulated results show that the achieved bandwidths, at the four operational frequency bands, are 0.6, 0.6, 1.8, and 1.5 GHz, respectively. Also, the radiation efficiencies calculated at the four operational frequencies are 86.5%, 87.5%, 89.2%, and 90.0%, respectively. The dimensions and the results concerning the performance of the proposed MIMO antennas are compared to those of other designs for MIMO antennas available in some recently published work.

1. INTRODUCTION

One of the essential demands for the future generations of mobile communications is the capability of the mobile handsets to transfer data with very high speed. A mobile handset antenna should have compact profile and simple structure [1, 2]. To meet the standards of long-term-evolution (LTE) and fifth generation (5G) of mobile communications [3] an antenna of handheld device should provide broadband operation, high data rate, and low power consumption. This recommends that a mobile handset antenna should be able to operate in the range of mm-wave of the electromagnetic spectrum to support the required data rates for the future applications. Moreover, due to size limitations, it is recommended that a mobile handset antenna is able to operate efficiently at multiple frequency bands in the mm-wave spectrum to support the applications of the forthcoming mobile generations [4, 5]. In the various situations, the antenna structure may be complicated as those having three-dimensional shape to operate efficiently in a single frequency band and to perform some function in special applications [6, 7] and may include layers with high electromagnetic absorbance [8] to produce radiation patterns of desired shape. However, for mobile handsets, due to size and weight limitations, it is preferable to have planar antenna of simple-structure, multi-band operation and omnidirectional radiation patterns.

The design of a MIMO antenna system for operation in mobile handsets for the forthcoming generations of mobile communications faces many challenges. First of all, the MIMO antenna on a handset should be miniaturized due to space limitation. The second challenge is to get high isolation between the antenna elements in spite of the small area available for the antenna on the mobile handset. The third challenge is to get the MIMO antenna operational at multiple frequencies with

Received 1 January 2022, Accepted 31 March 2022, Scheduled 11 April 2022
* Corresponding author: Asmaa Elsayed Farahat (asmaa@eri.sci.eg).
The authors are with the Electronics Research Institute (ERI), Cairo, Egypt.

enough wideband at each frequency (multiple-band operation). The fourth challenge is to produce the required shape of the radiation patterns over the operational frequency bands. Also, it may be required for a MIMO antenna to provide many types of diversity such as the spatial, polarization and pattern diversities. One of the most important challenges of MIMO antenna design for mobile handset is to provide low envelop correlation coefficient (ECC) and high diversity gain (DG).

Various types of MIMO antenna systems for 5G mobile handsets, recently, have been designed in a lot of research articles. For example, in [9], compact microstrip line fed dual-band printed two-port and four-port MIMO antennas are proposed for wireless communications. In [10], a seven-port MIMO antenna system is proposed as a candidate for future mobile communications to operate at 37.5 GHz. A cross-polarized four-port dual-band MIMO antenna array is proposed in [11] to operate at 28 and 37.5 GHz for 5G communications. Each element of this MIMO system is composed of two identical patches. The work of [12] proposes a dual-band two-port MIMO antenna to operate at 28 and 38 GHz for 5G mobile applications. In [13], a planar dual-band (27/39 GHz) millimeter-wave two-port MIMO antenna is suggested for 5G mobile communications. The work of [14] introduces a compact four-port MIMO antenna with high-isolation and single wideband for mm-Wave Applications. In [15] and [16], quad-band (28/45/51/56 GHz) two-port and four-port MIMO antenna systems are proposed for 5G mobile communications. The work of [17] proposes a dual-band (28/38 GHz) four-port MIMO antenna system for 5G mobile communications for efficient Estimation of the directional of arrival in noisy communication channels. In [18] and [19], dual-Band (28/38 GHz) cross-polarized four-port MIMO antenna systems composed of high-gain Yagi-Uda antenna with corrugated radiators and enhanced reflectors is proposed to provide spatial, polarization and pattern diversities for 5G mobile communications. [20] and [21] introduced MIMO antennas using conformal arrays for the fifth generation wireless communication systems.

In this work, compact-size quad-band four-port MIMO antenna systems are proposed to operate in the millimetric-wave bands (28/43/52/57 GHz) for the forthcoming generations of mobile communications. The proposed MIMO antennas provide various types of antenna diversity to enhance the performance of mobile communication systems. A co-polarized four-port MIMO antenna system with high isolation among the antenna elements is proposed to provide spatial polarization and another cross-polarized four-port MIMO antenna is proposed to provide both spatial and polarization diversities.

The present paper is organized as follows. Section 2 is concerned with the description of the quad-band single-element antenna that is suggested to construct the proposed MIMO antenna systems. Section 3 provides a detailed explanation of the process of antenna fabrication and the techniques used for experimental measurements. Section 4 gives a complete description of the two types of four-port MIMO antennas proposed in the present work. Section 5 summarizes the achievements of the present paper and gives some comparisons with other recently published research work. Finally, Section 6 gives the most important conclusions of the present work.

2. DESIGN OF THE QUAD-BAND SINGLE-ELEMENT ANTENNA

A hexagonal patch antenna is designed with the dimensional parameters set to the proper values so as to get the hexagonal patch antenna principally operational at 28 GHz. These dimensional parameters are the side length of the hexagonal patch (equivalently, the patch radius), the inset length, and the width of the notches which are cut on the sides of the feeding line for inset feed. In order to get the antenna resonant at higher frequency bands, additional printed elements are added to the driven hexagon patch. These additional patches improve the impedance matching at the higher frequency bands. They can be either capacitively or inductively loaded to the driven patch. In the proposed design, a secondary capacitive parasitic patch is reactively loaded to the original hexagonal patch. Also to minimize the driven patch dimensions, the parts of the patch with insignificant current magnitude are cut away. The dimensions of the modified patch and the parasitic element are set so that the printed structure has multiple resonances at the desired frequencies and improved impedance matching (assuming $50\,\Omega$ source). Extensive parametric study is performed to select the appropriate dimension. The final design of the proposed patch antenna with the dimensional parameters is shown in Figure 1. The antenna is designed to be printed on Rogers RO3003 substrate of dimensions $W \times L = 10{\times}18\,\text{mm}^2$ of 0.25 mm thickness, dielectric constant $\varepsilon_r = 3$, and loss tangent $\tan\delta = 0.001$. The substrate has a solid ground

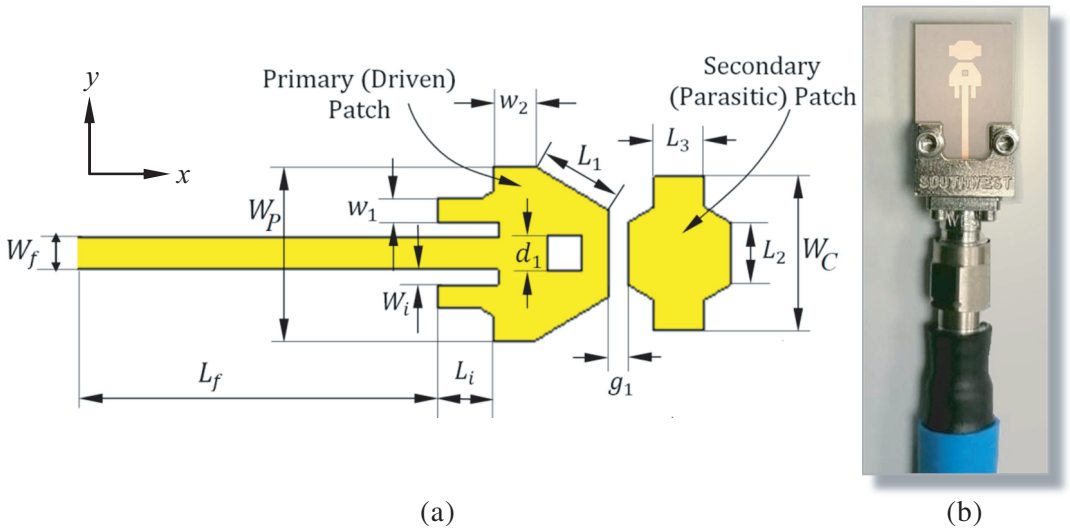

(a) (b)

Figure 1. The quad-band millimetric-wave antenna proposed for MIMO antenna systems. (a) Geometry of the printed antenna. (b) Fabricated antenna prototype is connected to end launcher and coaxial cable for measurements.

plane to reduce the back radiation of the antenna. The printed antenna is fed through a microstrip line of length $L_f = 10\,\text{mm}$. The width of the microstrip line is set to $W_f = 0.63\,\text{mm}$ to get its characteristic impedance equal to $50\,\Omega$. An inset feed is used to match the antenna impedance to $50\,\Omega$. The inset length is $L_i = 1.23\,\text{mm}$ and width of each slot made on the sides of the feeding line for the inset feed is $W_i = 0.3\,\text{mm}$. The remaining dimensions are listed in Table 1. This antenna can be viewed as composed of two patches; the primary patch is directly fed through a microstrip line, whereas the secondary patch can be considered as a parasitic radiator that is excited through capacitive coupling with the primary patch.

Table 1. Dimensions of the quad-band printed antenna proposed for the MIMO antenna system.

Dimension	$\mathbf{L_1}$	$\mathbf{L_2}$	$\mathbf{L_3}$	$\mathbf{w_i}$	$\mathbf{w_1}$	$\mathbf{w_2}$	$\mathbf{d_1}$	$\mathbf{g_1}$	$\mathbf{W_P}$	$\mathbf{W_C}$
Value (mm)	1.7	1.2	1	0.3	0.45	0.85	0.7	0.38	3.4	3.0

3. PROTOTYPE FABRICATION AND MEASUREMENT TECHNIQUES

In the present work, some of the most important results of electromagnetic simulation performed to investigate the proposed antennas are to be verified using the experimental measurements. For this reason, it is required to fabricate prototypes of the various MIMO antennas investigated in the present work. The experimental work involves the performance assessment of the single-element antenna itself through the measurement of the impedance, gain and radiation patterns. Also, the experimental work involves the measurement of self and mutual S-parameters among the multiple ports of the proposed types of MIMO antennas. The process of antenna fabrication and the techniques used for experimental measurement are described in this section.

3.1. Antenna Prototype Fabrication

A prototype for the quad-band single antenna has been fabricated as well as two types of four-port MIMO antennas proposed in the present work for the purpose of experimental investigation. The fabricated prototypes are shown in Figure 2. The purpose of fabrication is to evaluate the performance of the proposed quad-band printed antenna and the proposed two types of the MIMO antennas through

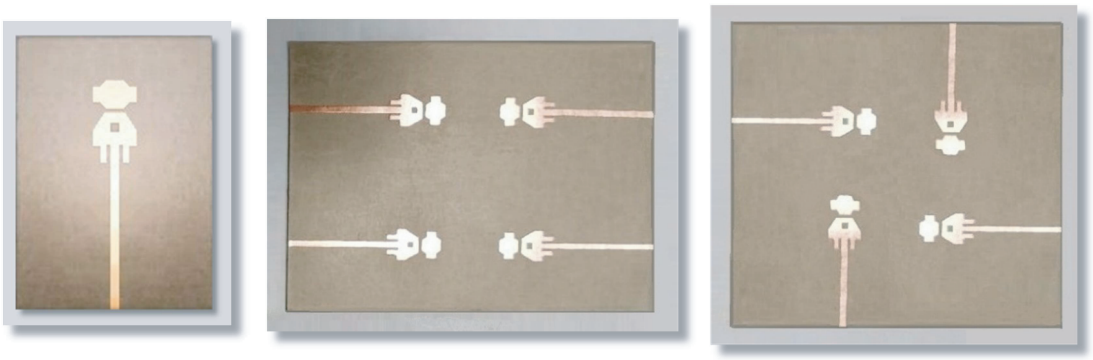

(a) (b) (c)

Figure 2. Fabricated prototypes of the various millimetric-wave antennas investigated in the present work. (a) Single-element antenna. (b) Co-polarized four-port MIMO antenna. (c) Cross-polarized four-port MIMO antenna.

experimental measurements of the antenna impedance, gain and radiation patterns. The technology of photolithography has been used for fabrication. In this technique, a photo-mask of the planar antenna layout is, first, prepared where the regions corresponding to copper portions are drawn as opaque black areas whereas the regions corresponding to bare portions are left transparent. A double-face copper-coated substrate is covered with photoresist material by spin coating. The faces of the substrate are, then, covered with the photo-mask of the planar antenna layout that has been prepared as described above. As the proposed antennas have solid ground structure without any defects, the photo-mask is placed just on the top face of the substrate, which is then exposed to an intense UV light to remove the photoresist material coat from areas that should be free from copper. The last stage of the photolithography is the etching process, where a liquid chemical (ferrous chloride) is used to remove the copper from the top face of the substrate in the areas that have been freed from the photoresist cover.

3.2. Measurement Techniques for Experimental Assessment of the Proposed Antennas

The main parameters required to be experimentally evaluated are the self S-parameters for each port in a MIMO antenna and the mutual S-parameters between each pair of ports. The self S-parameter can be used to evaluate the input impedance at each one of the multiple antenna ports. On the other hand, the mutual S-parameters can be used to evaluate the ECC and DG for each pair of the antenna ports. The gain and radiation patterns are measured at the frequencies of interest. The techniques of measuring the gain and radiation patterns are described in detail. The equipment, tools, and components used for experimental measurements are listed in Table 2.

The VNA is used to measure the antenna input impedance and, hence, the reflection coefficient $|S_{11}|$ over the frequency range 20–60 GHz. The VSG-E8267D and VSA-N9010A are used to measure the radiation patterns at 28 GHz using the reference horn antenna A-Info LB018400 and at 43 GHz using the reference horn antenna A-Info LB-12-10-A. The radiation patterns at 52 and 56.5 GHz are measured using the VNA-ZA67 and the reference horn antenna A-Info LB-12-10-A.

3.2.1. Measurement of Self and Mutual Scattering Parameters

The VNA of Rhode and Schwartz model ZVA67 is used for measuring the frequency response of the self and mutual S-parameters for multiple-port antenna systems. An example for the experimental setup used for measurement of two-port MIMO antenna is shown in Figure 3. In this case, the self S-parameters S_{11} and S_{22} and the mutual S-parameters S_{21} and S_{12} are required to be measured over the frequency band 20–60 GHz. Two 1.85 mm end-launch connectors and flexible coaxial cables are used for linking the antenna ports to ports 1 and 2 of the VNA as shown in the figure. For MIMO antenna systems having more than two ports, each port that is not connected to the VNA should be connected

Table 2. List of the devices used for experimental measurements of the antenna input impedance and radiation characteristics.

Device	Model	Frequency Range
Vector Network Analyzer (VNA)	Rhode&Schwartz ZVA67	10 MHz–67 GHz
Vector Signal Generator (VSG)	Agilent E8267D	100 kHz–44 GHz
Vector Signal Analyzer (VSA)	Agilent N9010A	10 Hz–44 GHz
Reference Horn Antenna (20 dBi-Gain)	A-Info LB018400	18–40 GHz
Reference Horn Antenna (20 dBi-Gain)	A-Info LB-12-10-A	40–60 GHz
2.4 mm Female End-Launch Connector	Southwest 1492-04A-8	Up to 50 GHz
1.85 mm Female End-Launch Connector	Southwest 1892-04A-8	Up to 67 GHz
Male/Male Coaxial Cables	Rhode&Schwartz ZV-Z196	Up to 75 GHz
VNA Calibration kit	Rhode&Schwartz ZV-Z218	10 MHz–67 GHz

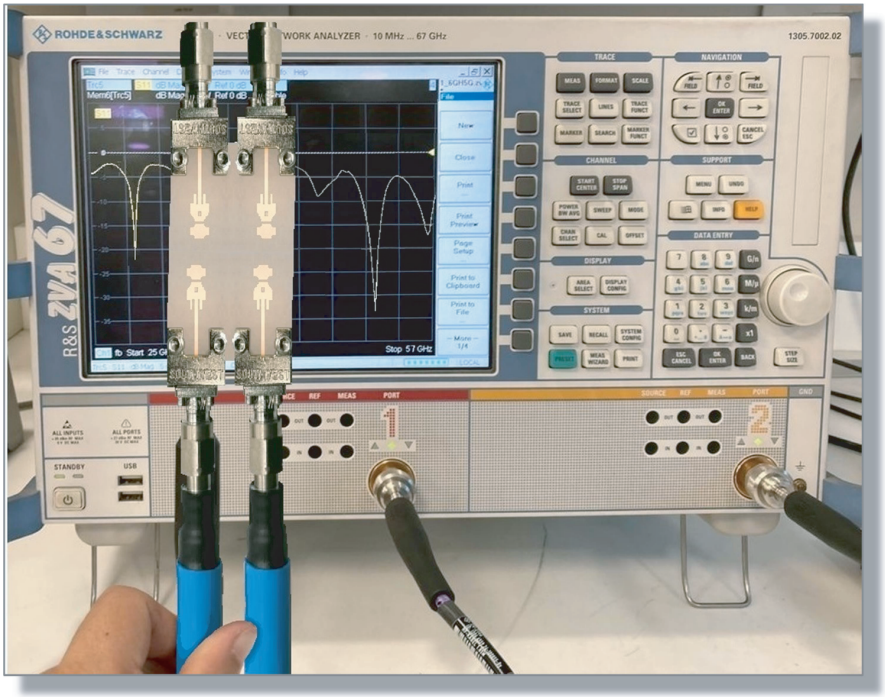

Figure 3. Measurement of the reflection coefficient $|S_{11}|$ of the proposed quad-band patch antenna: (a) The fabricated prototype is connected to the end launcher; (b) The antenna is connected to the VNA of Rhode and Schwartz model ZVA67.

to a broadband matched load during the measurements. The VNA is prepared for measurement by setting the start and stop frequencies to 20 GHz and 60 GHz, respectively. The full two-port calibration procedure for measuring the four S-parameters (S_{11}, S_{22}, S_{21}, and S_{12}) is then applied using the standard mechanical calibration kit model ZV-Z218.

3.2.2. Measurement of the Gain and Radiation Patterns

For gain and normalized radiation pattern measurement, the reference horn antenna boresight is directed towards the antenna under test (AUT) as shown in Figure 4. The AUT is mounted on a rotator that can be used to rotate the antenna about its axis in its horizontal and elevation planes. Let the distance

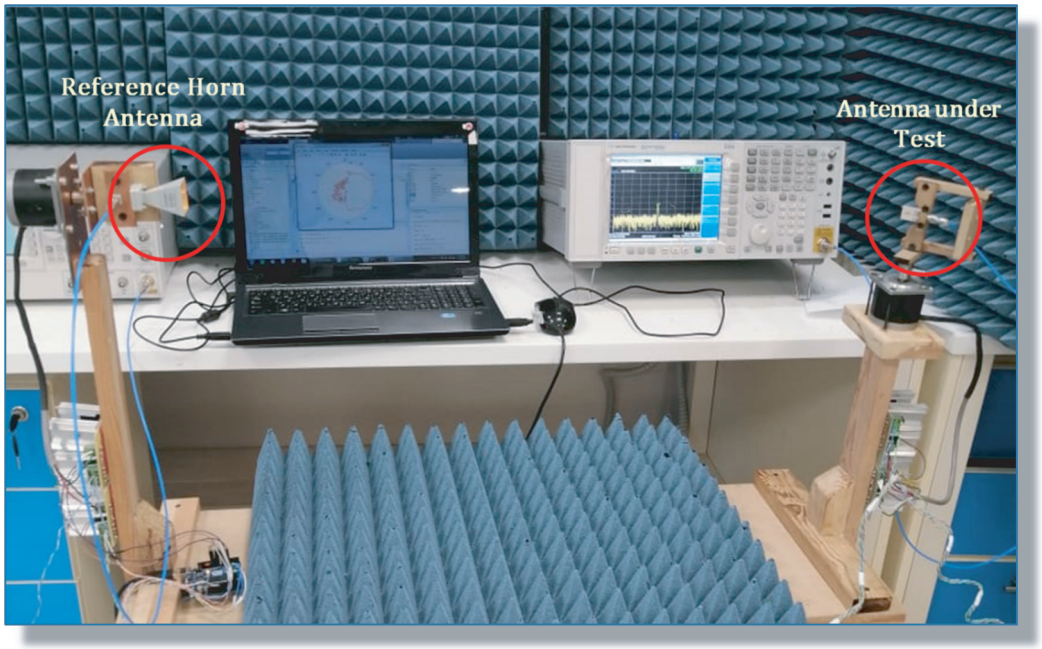

Figure 4. Measurement of the far-field and gain patterns of the proposed MIMO antennas using the VSG and VSA.

between the reference horn antenna and the AUT be D. It should be noted that, during gain and pattern measurement, the AUT should be in the far field region of the reference horn antenna. The far-field distance can be calculated according to the formula $2L^2/\lambda$ where L is largest dimension of the antenna and λ is the shortest wavelength during measurement. As the largest dimension of the reference horn antenna is 5 cm and the highest frequency is 60 GHz ($\lambda = 0.5$ cm), the far-field distance, according to the above formula, is 100 cm. For measurement, the AUT is connected to port 1 of the VNA, and the reference horn antenna is connected to port 2 through flexible coaxial cables of low insertion loss. Let the positive z-axis be in the outward direction normal to the plane of the printed antenna and (θ, ϕ) be angular dimensions of the corresponding spherical coordinate system. The power density at the reference receiving antenna can be expressed as follows

$$\frac{|E_R(\theta,\phi)|^2}{2\eta} = \frac{P_T}{4\pi D^2} G_T(\theta,\phi) \tag{1}$$

where P_T is the transmitted power; $E_R(\theta,\phi)$ is the electric field at the receiving antenna when the transmitting antenna is oriented in the direction (θ,ϕ); $G_T(\theta,\phi)$ is the gain of the transmitting antenna (AUT) in the same direction; and $\eta = 120\pi\,\Omega$ is the intrinsic impedance of free space.

The power received by the reference horn antenna when the transmitting antenna is oriented in the direction (θ,ϕ) can be expressed as follows.

$$P_R(\theta,\phi) = \frac{|E_R(\theta,\phi)|^2}{2\eta} A_R = \frac{P_T}{4\pi D^2} G_T(\theta,\phi) \frac{\lambda^2}{4\pi} G_R \tag{2}$$

where $A_R = \frac{\lambda^2}{4\pi} G_R$ and G_R are, respectively, the effective area and gain of the reference horn antenna in the boresight direction.

Using Eq. (2), the gain of the AUT can be expressed as follows.

$$G_T(\theta,\phi) = \left(\frac{4\pi D}{\lambda}\right)^2 \frac{P_R(\theta,\phi)}{P_T} G_R \tag{3}$$

If the gain pattern is measured using the measurement setup that employs the VSG and VSA as shown in Figure 3, $P_R(\theta,\phi)$ can be obtained from the readings of the VSA when the AUT is oriented in the direction (θ,ϕ), and P_T is the transmitted power set by the control of the VSG.

If the VNA is used for measurement, the ratio $P_R(\theta,\phi)/P_T$ can be obtained from the S-parameter $S_{21}(\theta,\phi)$ when the transmitting antenna is oriented in the direction (θ,ϕ) as follows.

$$\frac{P_R(\theta,\phi)}{P_T} = |S_{21}(\theta,\phi)|^2 \tag{4}$$

Thus, the gain pattern $G_T(\theta,\phi)$ of the AUT can be calculated from the readings $S_{21}(\theta,\phi)$ (obtained by the VNA) as follows.

$$G_T(\theta,\phi) = \left(\frac{4\pi D}{\lambda}\right)^2 G_R\,|S_{21}(\theta,\phi)|^2 \tag{5}$$

The normalized radiation pattern of the AUT can be obtained as follows. The electric field at the receiving antenna when the AUT is oriented in the direction (θ,ϕ) can be obtained as follows.

$$|E_R(\theta,\phi)| = \sqrt{2\eta P_R(\theta,\phi)} \tag{6}$$

Substituting from (4) into (6), the following expression is obtained.

$$|E_R(\theta,\phi)| = \sqrt{2\eta P_T}\,|S_{21}(\theta,\phi)| \tag{7}$$

Thus, the normalized radiation pattern can be obtained from the readings of the VNA as follows.

$$\left|\hat{E}_R(\theta,\phi)\right| = \frac{|E_R(\theta,\phi)|}{|E_R|_{\max}} = \frac{|S_{21}(\theta,\phi)|}{|S_{21}|_{\max}} \tag{8}$$

where $|E_R|_{\max}$ is the maximum of $|E_R(\theta,\phi)|$ over all the spatial directions (θ,ϕ) at the operating frequency, and $|S_{21}|_{\max}$ is the maximum of $|S_{21}(\theta,\phi)|$ at the same frequency.

4. CHARACTERISTICS OF THE QUAD-BAND SINGLE-ELEMENT ANTENNA

The millimetric-wave antenna presented in Section 2 with the geometry shown in Figure 1 and the dimensional parameters listed in Table 1 is used to construct various configurations of four-port MIMO antenna systems with various types of diversity proposed for the handsets of the forthcoming generations of mobile communications. Accordingly, it is important to investigate the characteristics of this antenna through electromagnetic simulation and laboratory measurements. Figure 5 presents the dependence of the scattering parameter $|S_{11}|$ at the antenna port as obtained by both simulation and experimental measurements. It is shown that the antenna has four operational millimetric-wave frequency bands at

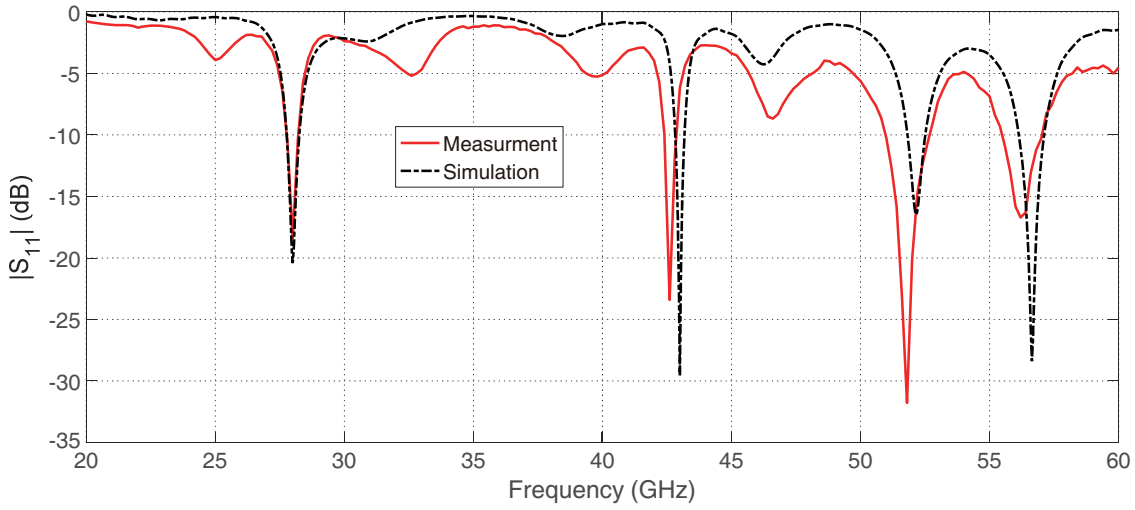

Figure 5. Dependence of the reflection coefficient $|S_{11}|$ on the frequency for the proposed quad-band patch antenna.

which the antenna is matched to 50 Ω feeder, and hence, the return loss is very low. The operational frequency bands are 28, 43, 52, and 57 GHz. Fortunately the four frequencies are distributed over very important range of the millimetric-wave which makes this antenna a promising candidate for future mobile applications.

The radiation patterns produced by this antenna at the four frequencies are presented in Figures 6–9 where the experimentally evaluated patterns in both the E- and H-planes of the antenna show good agreement with those evaluated through electromagnetic simulation. The radiation patterns at the four frequencies seem to be appropriate for constructing MIMO systems for mobile handsets for both short-range and long-range mobile communications.

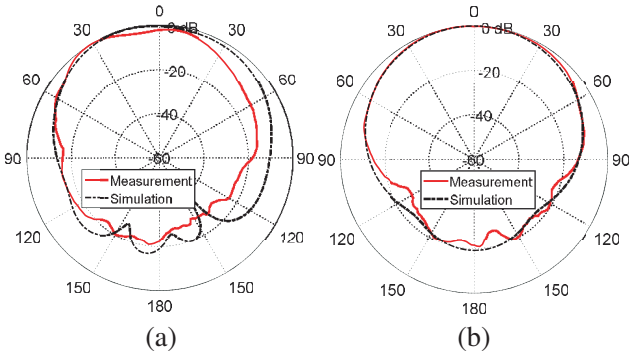

Figure 6. Radiation patterns of the proposed quad-band patch antenna at 28 GH in the elevation planes. (a) $\phi = 0°$ and (b) $\phi = 90°$.

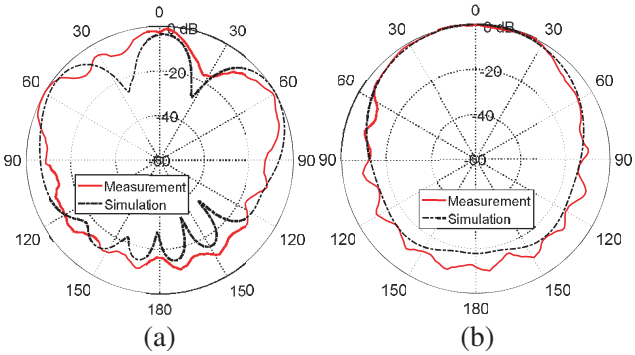

Figure 7. Radiation patterns of the proposed quad-band patch antenna at 43 GHz in the elevation planes. (a) $\phi = 0°$ and (b) $\phi = 90°$.

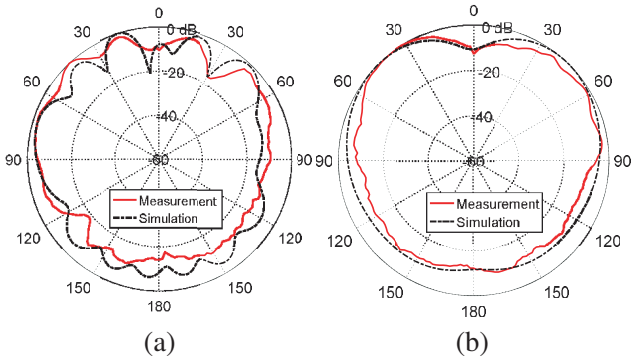

Figure 8. Radiation patterns of the proposed quad-band patch antenna at 52 GH in the elevation planes. (a) $\phi = 0°$ and (b) $\phi = 90°$.

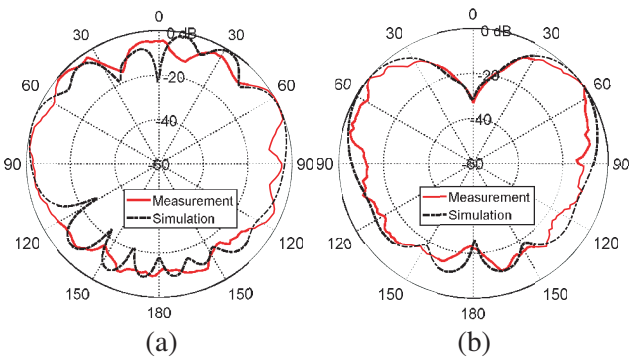

Figure 9. Radiation patterns of the proposed quad-band patch antenna at 56.5 GHz in the elevation planes. (a) $\phi = 0°$ and (b) $\phi = 90°$.

5. QUAD-BAND FOUR-PORT MIMO ANTENNA SYSTEM FOR SPATIAL AND POLARIZATION DIVERSITY

Four-port MIMO antenna system on mobile handsets enhances the performance of mobile communications. The quad-band presented antenna introduced in Section 2 can be used to construct such MIMO antennas to provide both spatial and polarization diversity. In the following subsections two types of four-port MIMO antenna are proposed. The first type has its four antenna elements co-polarized and achieve spatial diversity with high DG. The other type is cross-polarized MIMO antenna that can provide both spatial and polarization diversity.

5.1. Co-polarized Four-Port MIMO Antenna for Spatial Diversity

Four elements of the printed antenna introduced in Section 2 can be used to construct quad-band four-port MIMO antenna system as shown in Figure 10. The four antennas are y-oriented, and hence, feeding the MIMO antenna at any of the four ports will produce vertically polarized electric field. However, due to the large number of ports, this co-polarized four-port MIMO antenna system will provide spatial diversity gain. That is much higher than that of co-polarized two-port MIMO antennas.

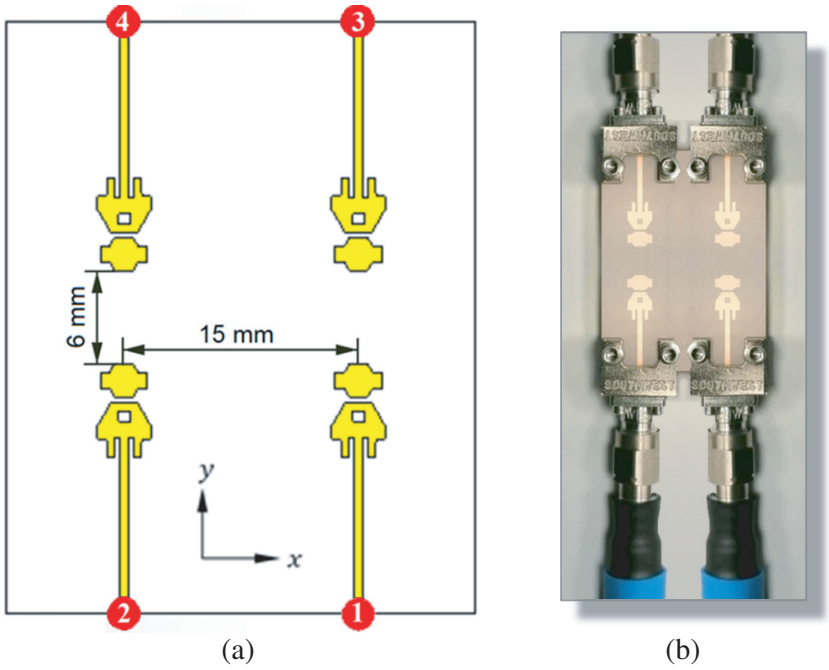

Figure 10. Quad-band co-polarized four-port MIMO antenna system (total dimensions $42 \times 20\,\text{mm}^2$) proposed for mobile handsets. (a) Geometric model for simulation. (b) Fabricate prototype of the MIMO antenna system.

5.1.1. Design and Fabrication of Co-Polarized Four-Port MIMO Antenna

The co-polarized four-port MIMO antenna has the design shown in Figure 10. Excluding the feeding microstrip lines, the outer dimensions of this MIMO antenna are $20 \times 20\,\text{mm}^2$. The length of each feeding line is arbitrary and will not affect the antenna performance at the four operational frequencies since the characteristic impedance is $50\,\Omega$ and the antenna elements are well-matched at the four frequencies.

The prototype shown in Figure 10(b) is fabricated using the photo lithographic technique as described in Section 3.1. for measuring the self and mutual S-parameters using the two-port VNA model ZVA-67, each pair of ports of this MIMO antenna is connected to the VNA through 1.85 mm end-launch connectors whereas the other two ports are terminated with broadband matched loads through the same type of end-launch connectors as shown in Figure 10(b).

5.1.2. Mutual Coupling among the Four Antenna Ports

One of the most important performance indicators of a MIMO system is the level of mutual coupling among the multiple antenna elements. For satisfactory performance, the self S-parameters S_{11} and S_{22} should be preserved close to that of a single (isolated) antenna element. On the other hand, the mutual S-parameters between the antennas of each pair of the four ports should be of very low magnitudes.

The prototype of the proposed quad-band four-port MIMO antenna system, shown in Figure 10, is subjected to experimental assessment of its performance. The VNA Rhode and Schwartz model ZVA67

is used for measuring the frequency response of the reflection coefficients S_{21}, S_{43}, S_{31}, S_{42}, S_{41}, and S_{32}. Four 1.85 mm end-launch connectors from Southwest Microwave Incorporation are used for connecting two of the MIMO antenna ports to the VNA ports 1 and 2 whereas the other two ports of the MIMO antenna are connected to matched (50 Ω) loads as shown in Figure 3.

As shown in Figure 11, the behavior of each of the self S-parameters, $|S_{11}|$, $|S_{22}|$, $|S_{33}|$, and $|S_{44}|$ of the co-polarized four-port MIMO antenna with changing the frequency, is almost identical to that of the single-element antenna. On the other hand, the mutual S-parameters $|S_{21}|$, $|S_{31}|$, $|S_{41}|$, $|S_{32}|$, $|S_{42}|$, and $|S_{43}|$ are all of very low magnitudes over the entire frequency range (20–60) GHz. Thus, both self and mutual S-parameters indicate very low mutual coupling among the four antenna elements. Due to the geometrical symmetry of the co-polarized four-port MIMO antenna presented in Figure 10, it is clear that $|S_{21}| = |S_{43}|$, $|S_{31}| = |S_{42}|$, and $|S_{32}| = |S_{41}|$.

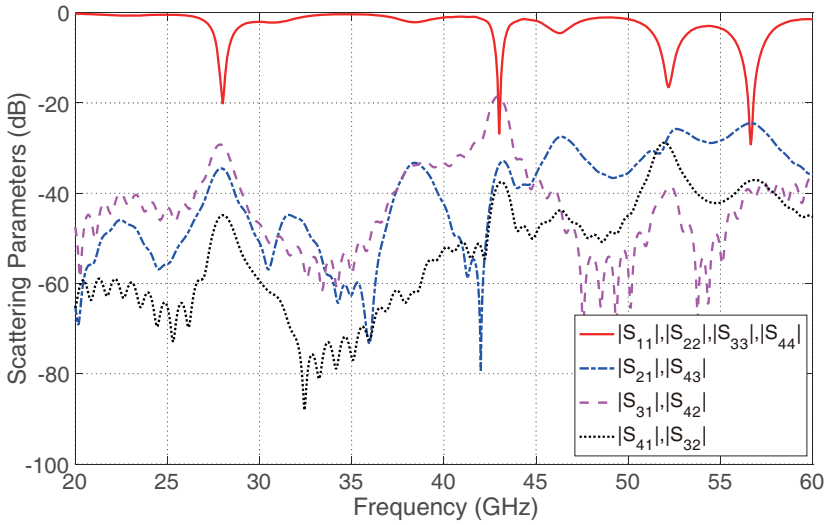

Figure 11. Frequency dependence of the self and mutual scattering parameters of the co-polarized four-port MIMO antenna system presented in Figure 9.

For confirmation of the simulation results presented in Figure 11, the mutual S-parameters are measured experimentally using a setup like that described in Section 3.2.1. As shown in Figure 12, the measurements come in good agreement with the simulation results and both show very low mutual coupling among the antenna elements of the co-polarized four-port MIMO antenna.

5.1.3. Envelope Correlation Coefficient and Diversity Gain of the Co-Polarized Four-Port MIMO Antenna

The ECC and DG for each pair of ports of the co-polarized four-port MIMO antenna have their frequency dependencies shown in Figure 13 over the frequency range (20–60 GHz). The ECC is maintained below 0.01 at the four operational frequencies, and the DG is maintained above 9.9 irrespective of the exciting ports. This can be considered as a direct consequence of the low mutual coupling among the four antennas as demonstrated in Section 5.1.2. These results show that the proposed co-polarized four-port MIMO antenna, presented in Figure 10, is an excellent MIMO antenna that enhances the communications performance and provides four-operational millimetric-wave frequencies. Also, it has planar structure and occupies only $20 \times 20\,\text{mm}^2$ area (of the antenna regions). Moreover, it is simply fabricated and can be simply integrated to the circuits on-board of a mobile handset.

5.1.4. Radiation Patterns of the Co-Polarized Four-Port MIMO Antenna System

The co-polarized four-port MIMO antenna presented in Figure 10, produces the radiation patterns shown in Figures 14, 15, 16, and 17 when the MIMO antenna is excited at ports 1, 2, 3, and 4,

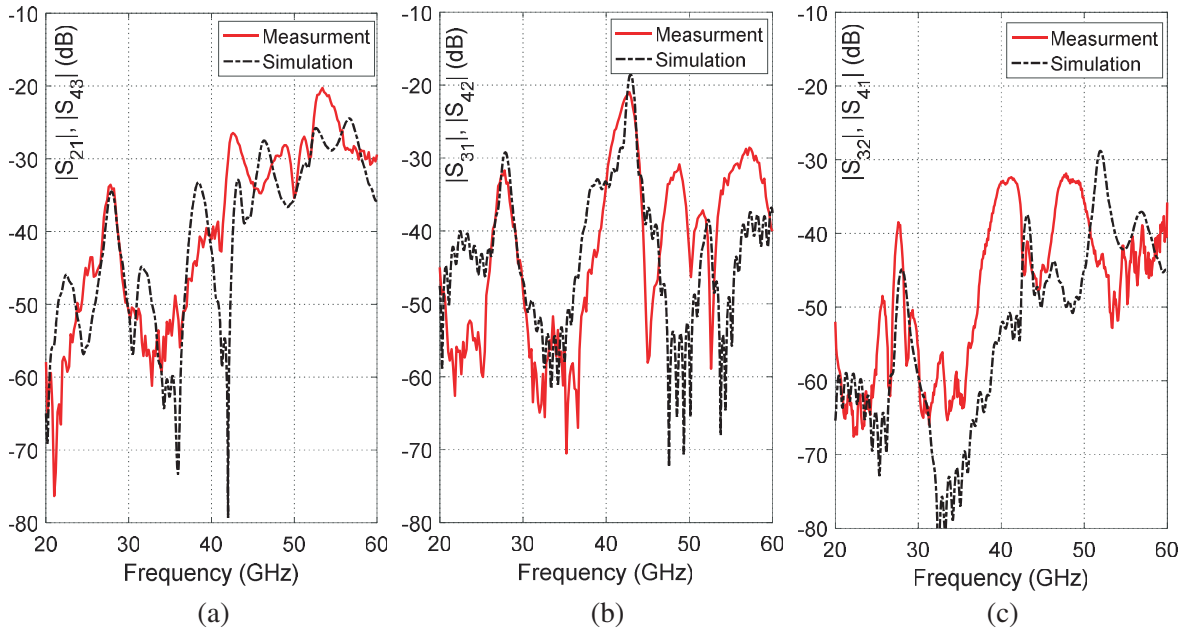

Figure 12. Frequency dependence of the magnitudes of the scattering parameters. (a) $|S_{21}|$, $|S_{43}|$, (b) $|S_{31}|$, $|S_{42}|$, (c) $|S_{32}|$, $|S_{41}|$, representing the different coupling coefficients for the co-polarized four-port MIMO antenna system.

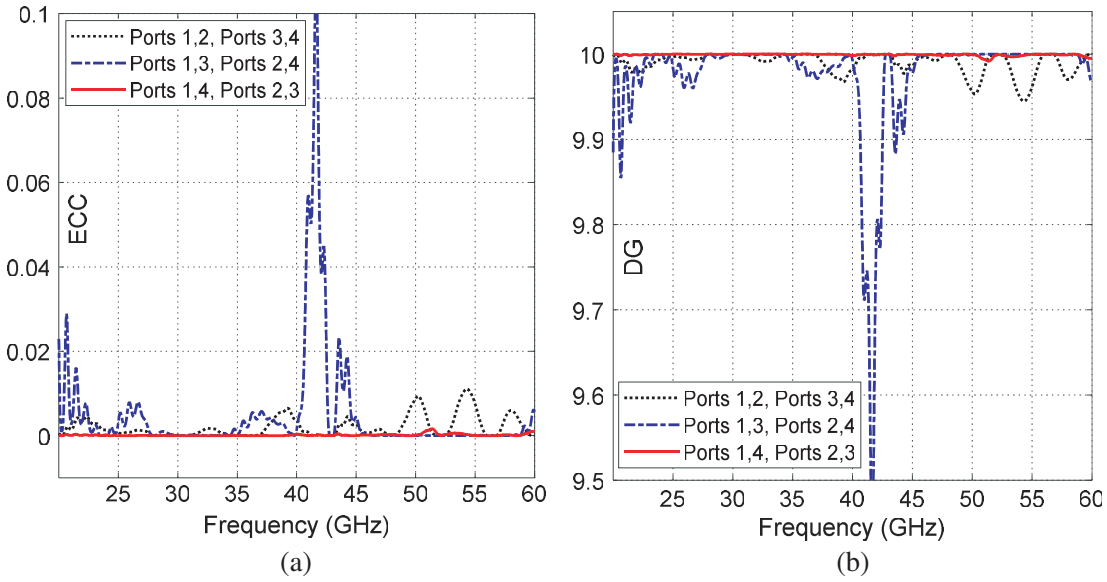

Figure 13. Frequency dependence of the (a) ECC, and (b) DG of the co-polarized four-port MIMO antenna system for the different pairs of exciting ports.

respectively. The produced radiation patterns in the elevation planes $\phi = 0°$ and $\phi = 90°$ at the four frequencies indicate that the radiation is almost omnidirectional in the azimuth plane. Thus, the proposed four-port MIMO antenna can be considered a good candidate for a mobile handset. However, it is recommended to use this MIMO antenna for long-range millimetric-wave communications at 20 and 43 GHz, and for short range communications at 53 and 57 GHz.

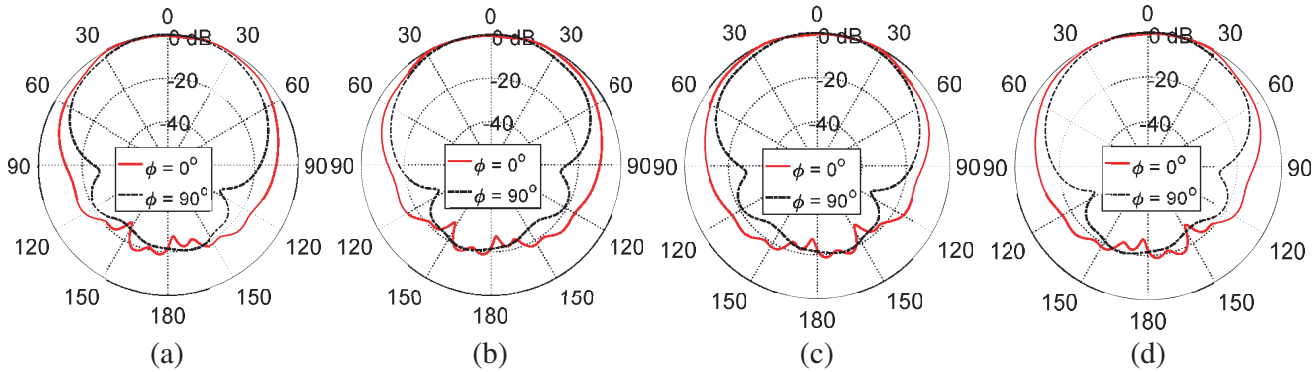

Figure 14. Radiation patterns in the elevation planes for the co-polarized four-port MIMO antenna system at 28 GHz when excited at (a) port 1, (b) port 2, (c) port 3, and (d) port 4.

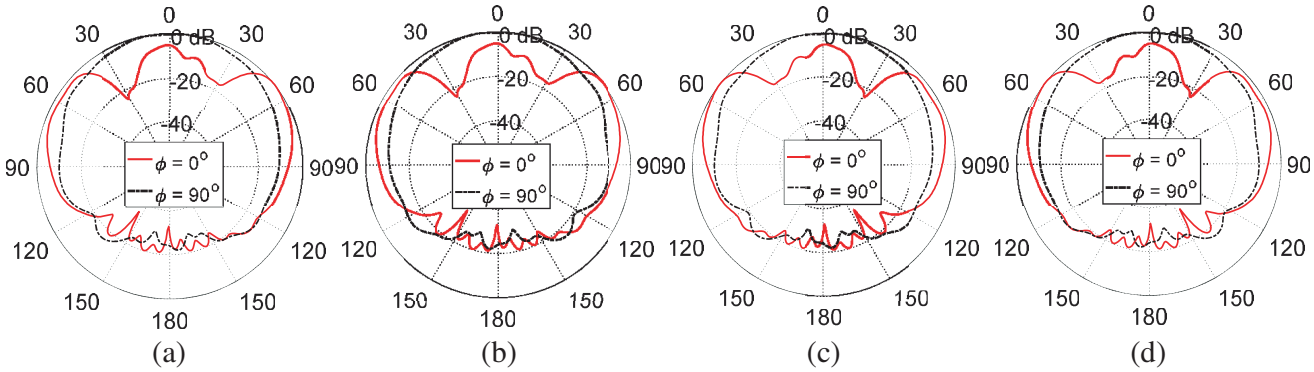

Figure 15. Radiation patterns in the elevation planes for the copolarized four-port MIMO antenna system at 43 GHz when excited at (a) port 1, (b) port 2, (c) port 3, and (d) port 4.

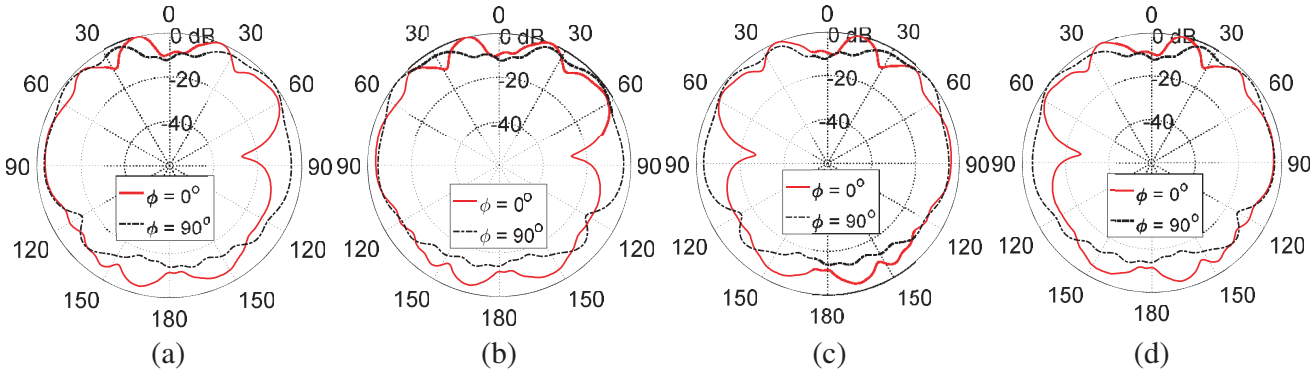

Figure 16. Radiation patterns in the elevation planes for the copolarized four-port MIMO antenna system at 52 GHz when excited at (a) port 1, (b) port 2, (c) port 3, and (d) port 4.

5.2. Cross-Polarized Four-Port MIMO Antenna for Spatial and Polarization Diversity

A MIMO antenna system that can provide both spatial and polarization diversities is shown in Figure 18. The proposed four-port MIMO antenna is constructed as two orthogonally oriented pairs of the single-element antenna introduced in Section 2.

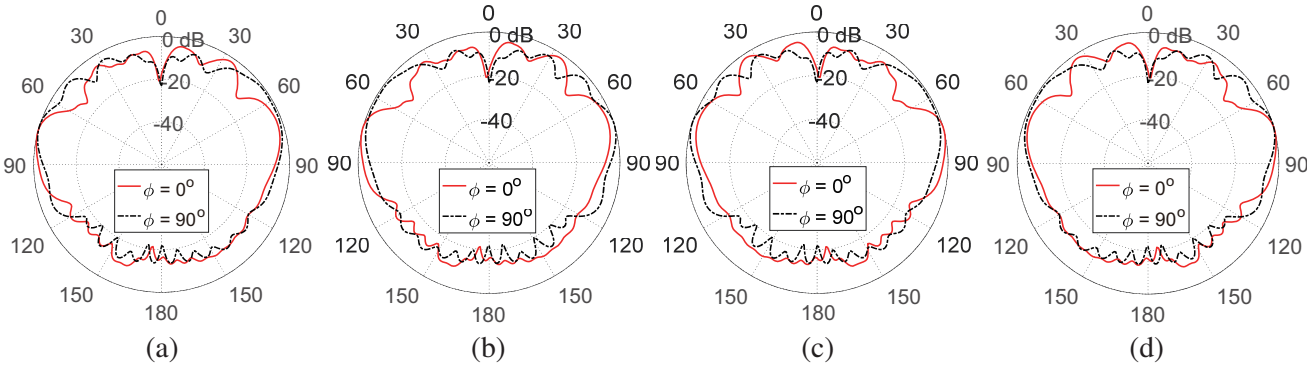

Figure 17. Radiation patterns in the elevation planes for the copolarized four-port MIMO antenna system at 57 GHz when excited at (a) port 1, (b) port 2, (c) port 3, and (d) port 4.

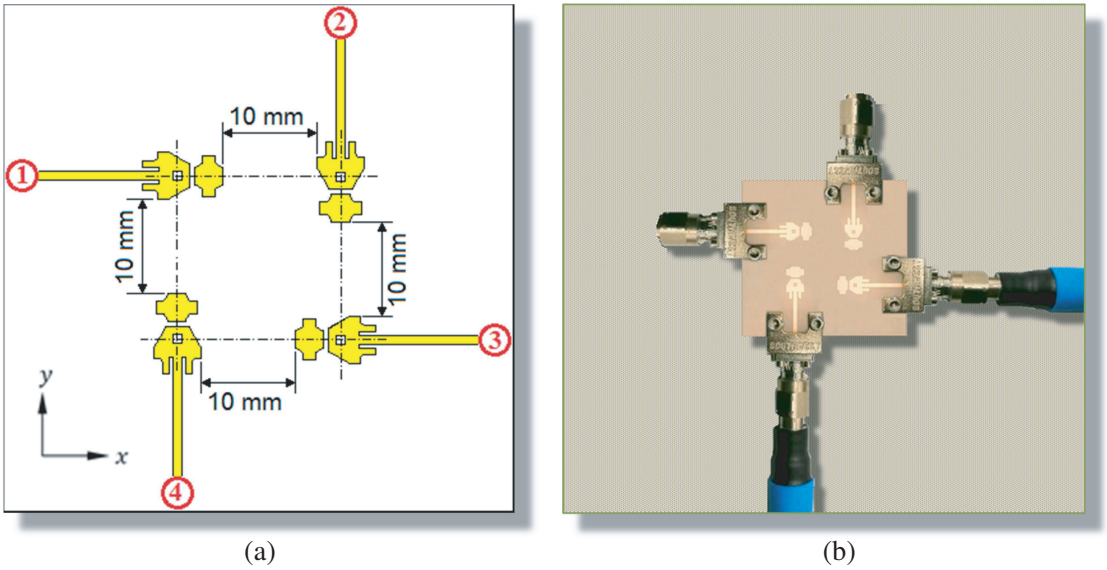

Figure 18. Quad-band cross-polarized four-port MIMO antenna system (total dimensions $42 \times 42\,\text{mm}^2$) proposed for mobile handsets. (a) Geometric model for simulation. (b) Fabricate prototype of the MIMO antenna system.

5.2.1. Design and Fabrication of Cross-Polarized Four-Port MIMO Antenna

The four-port MIMO antenna presented in Figure 18 is cross-polarized, i.e., a horizontally-polarized (x-oriented) electric field can be produced in the far zone when this MIMO antenna is excited at port 1 and/or port 3, whereas a vertically-polarized (y-oriented) electric field can be produced in the far zone when this MIMO antenna is excited at port 2 and/or port 4. Owing to the diagonal distance between antennas 1 and 3, spatial diversity can be realized. Thus the pair of antennas 1 and 3 provides horizontal polarization with spatial diversity. On the other hand, the pair of antennas 2 and 4 provides vertical polarization and spatial diversity due to the diagonal distance between the two antennas. In this way, the cross-polarized four-port MIMO antenna presented in Figure 18 is capable of providing both polarization and spatial diversities at the four operational frequencies 28, 43, 52, and 57 GHz.

5.2.2. Mutual Coupling among the Four Antenna Elements

The mutual effects among the four elements of the cross-polarized MIMO antenna presented in Figure 18 can be investigated by studying the self and mutual S-parameters over the frequency range 20–60 GHz.

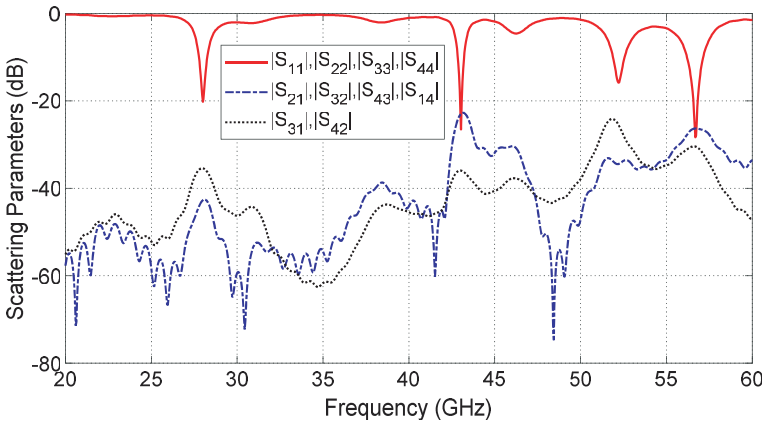

Figure 19. Frequency dependence of the self and mutual scattering parameters of the cross-polarized four-port MIMO antenna system.

As shown in Figure 19, the S-parameters $|S_{11}|$, $|S_{22}|$, $|S_{33}|$, and $|S_{44}|$ have almost the same frequency dependence as that of the single-element antenna which is presented in Figure 5. On the other hand, the S-parameters $|S_{21}|$, $|S_{31}|$, $|S_{41}|$, $|S_{32}|$, $|S_{42}|$, and $|S_{43}|$ are maintained below -23 dB over the entire frequency range. These results, concerned with self and mutual S-parameters, show that the mutual coupling among the four elements of the MIMO antenna is very weak.

Figure 20 shows comparisons between the simulation results and experimental measurements of the mutual S-parameters. These comparisons show that the measurements come in good agreement with the simulations results. It should be noticed that, due to the geometrical symmetry of the relative positions of some ports to each other, one has $|S_{21}| = |S_{41}| = |S_{32}| = |S_{43}|$, and $|S_{31}| = |S_{42}|$.

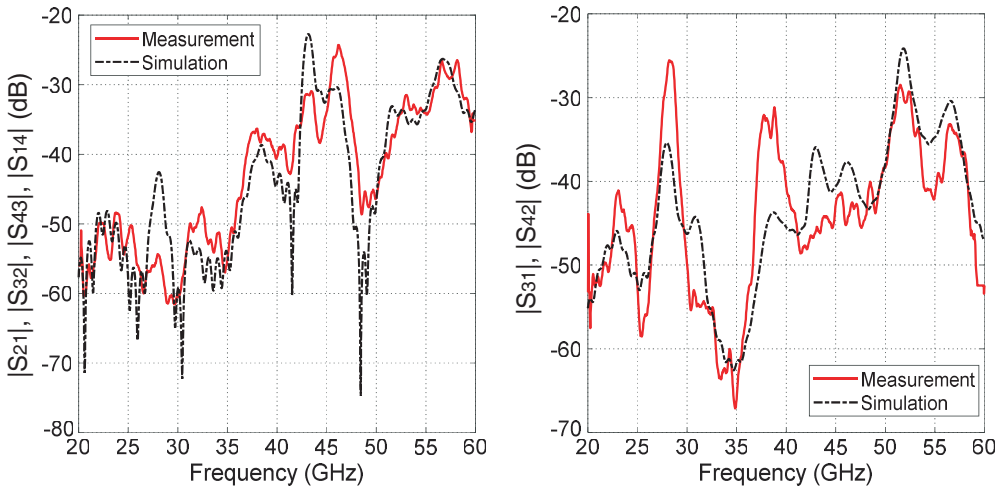

Figure 20. Frequency dependence of the magnitudes of the scattering parameters. (a) $|S_{21}|$, $|S_{32}|$, $|S_{43}|$, $|S_{14}|$, (b) $|S_{31}|$, $|S_{42}|$, representing the different coupling coefficients for the cross-polarized four-port MIMO antenna system.

5.2.3. Envelope Correlation Coefficient and Diversity Gain of the Cross-Polarized Four-Port MIMO Antenna

The orthogonal orientations of the antenna elements of the cross-polarized four-port MIMO antenna and the relatively large distance among them result in very low value of the ECC (for each pair of ports)

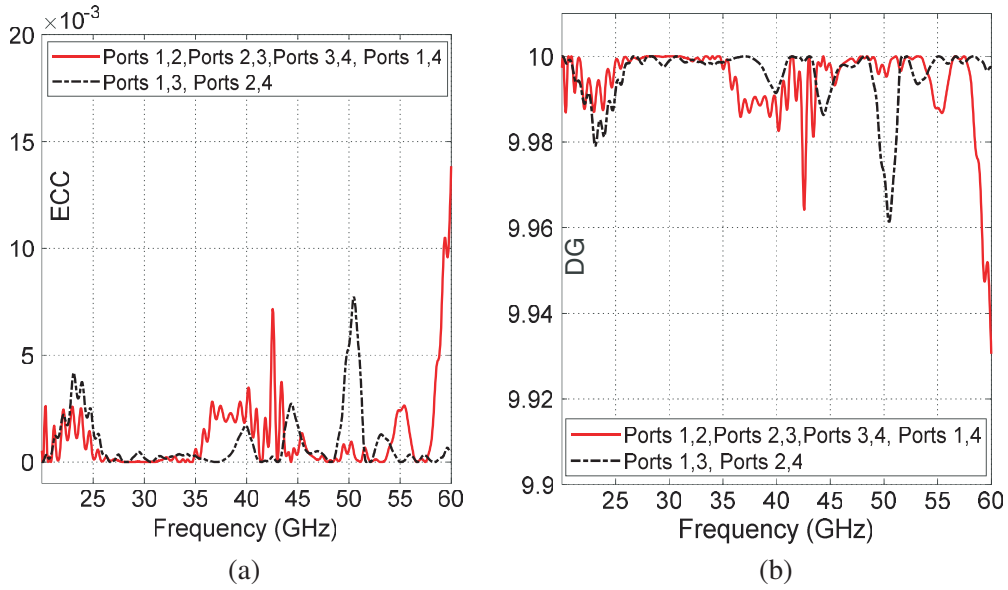

Figure 21. Frequency dependence of the (a) ECC and (b) DG of the cross-polarized four-port MIMO antenna system for the different pairs of exciting ports.

which is maintained below 0.0015 over the entire frequency range (20–60 GHz) as shown in Figure 21(a), and consequently, the DG is maintained above 9.92 over the same frequency range for each pair of ports as shown in Figure 21(b).

5.2.4. Radiation Patterns of the Cross-Polarized Four-Port MIMO Antenna System

The radiation patterns of the total radiated field at the frequencies 28, 43, 52, and 57 GHz are presented in Figures 22, 23, 24, and 25, respectively in the orthogonal planes $\phi = 0°$ and $\phi = 90°$ when the cross-polarized two-port MIMO antenna is excited at each port alone. From the radiation patterns in the two orthogonal planes it can be shown that the cross-polarized four-port MIMO antenna has omnidirectional radiation if the azimuth planes (θ = constant). This makes the antenna a promising candidate for mobile handset applications intended for the forthcoming generation of mobile communications.

For quantitative demonstration of the polarization diversity that can be provided by the cross-polarized four-port MIMO antenna proposed in the present work, the radiation patterns for the x-oriented and y-oriented components of the far electric field E_x and E_y respectively, at 28 GHz (for example), are plotted as shown in Figure 26 when the MIMO antenna is excited at each port alone. It is

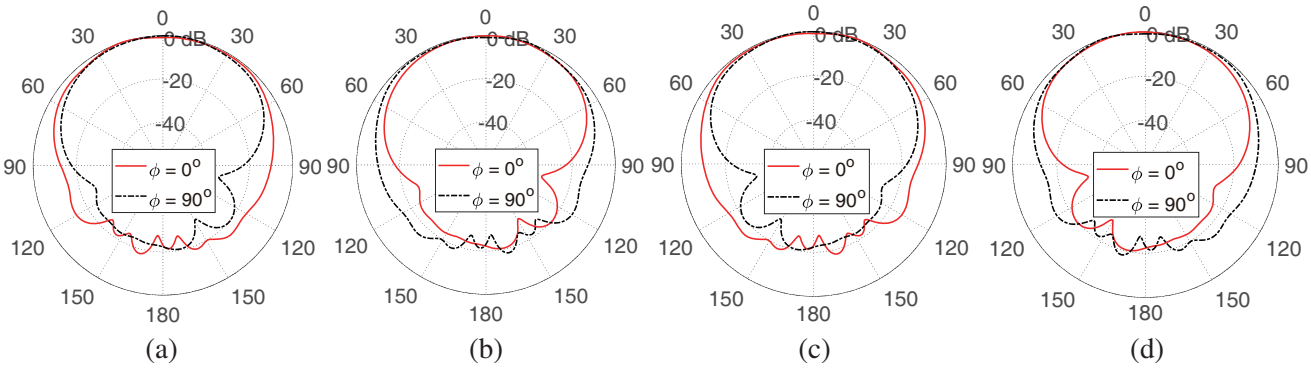

Figure 22. Radiation patterns in the elevation planes for the cross-polarized four-port MIMO antenna system at 28 GHz when excited at (a) port 1, (b) port 2, (c) port 3, and (d) port 4.

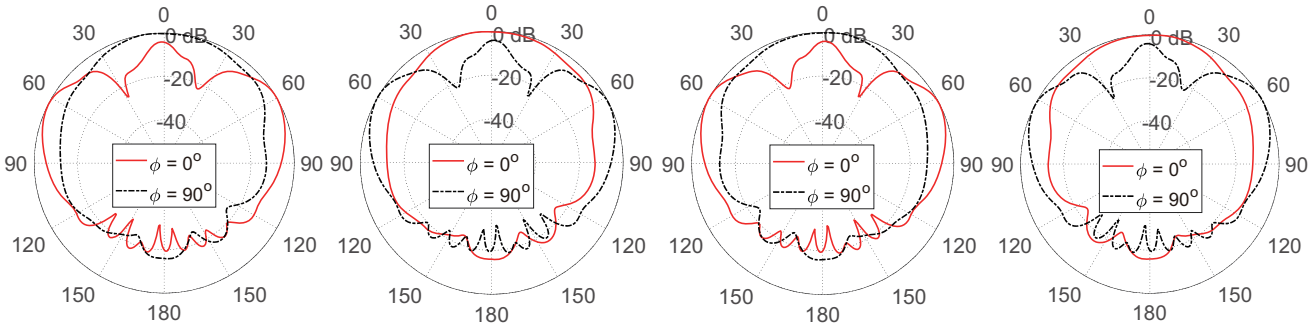

Figure 23. Radiation patterns in the elevation planes for the cross-polarized four-port MIMO antenna system at 43 GHz when excited at (a) port 1, (b) port 2, (c) port 3, and (d) port 4.

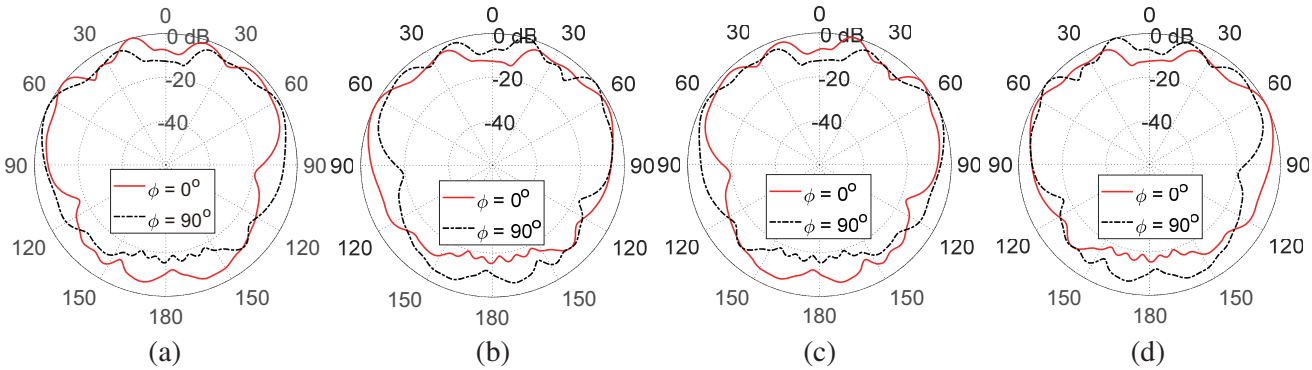

Figure 24. Radiation patterns in the elevation planes for the cross-polarized four-port MIMO antenna system at 52 GHz when excited at (a) port 1, (b) port 2, (c) port 3, and (d) port 4.

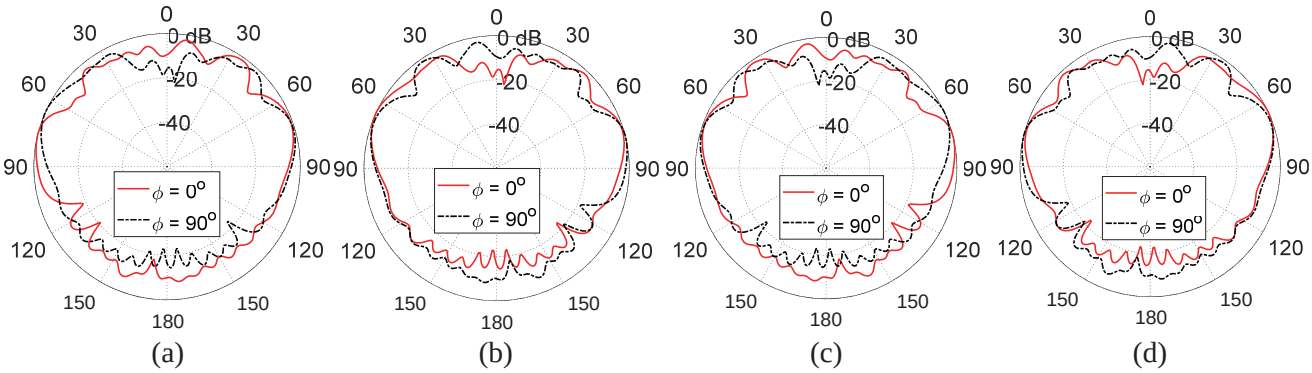

Figure 25. Radiation patterns in the elevation planes for the cross-polarized four-port MIMO antenna system at 57 GHz when excited at (a) port 1, (b) port 2, (c) port 3, and (d) port 4.

shown that the electric field dominated by an x-directed electric field when the MIMO antenna is excited at ports 1 and/or 3, and is dominated by a y-directed electric field when excited at ports 2 and/or 4. Thus, the proposed cross-polarized four-port MIMO antenna provides the polarization diversity required for enhancing the communication system performance.

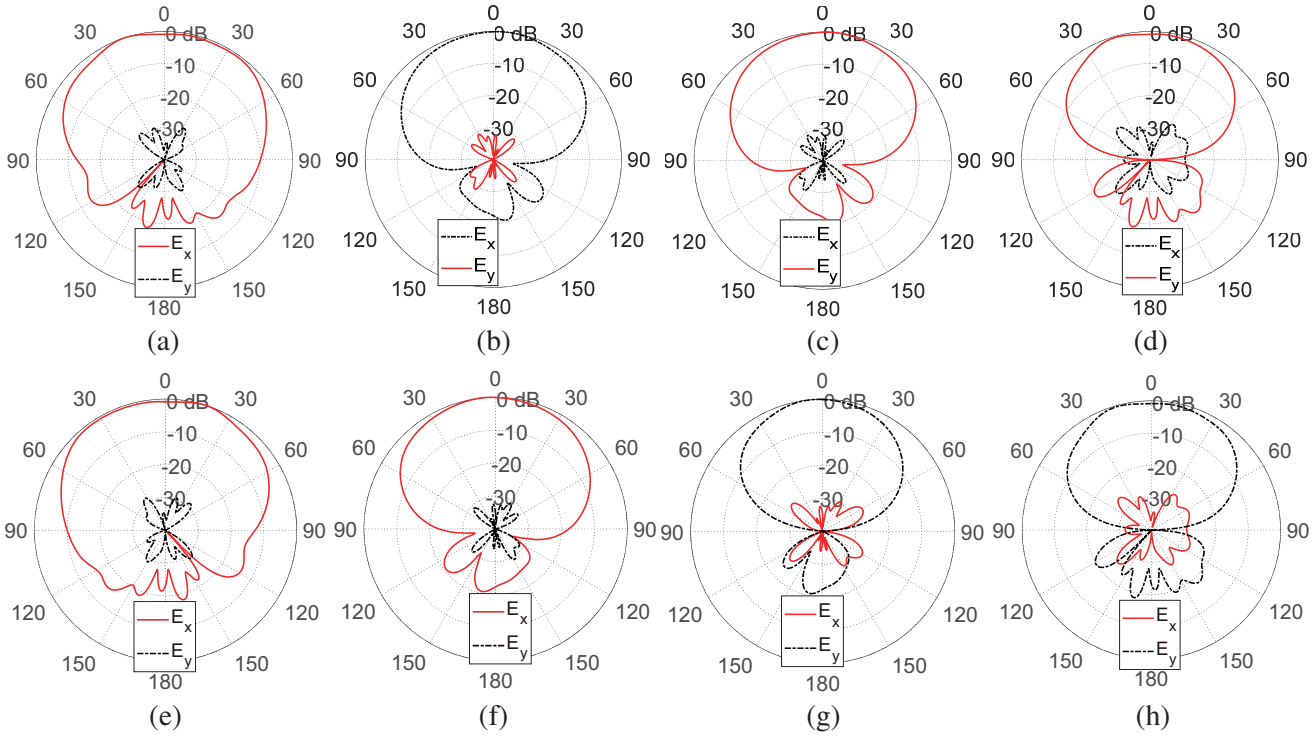

Figure 26. The radiation patterns of the horizontally polarized (x-oriented) and vertically polarized (y-oriented) electric field radiated from the cross-polarized four-port MIMO antenna system at 28 GHz in two orthogonal elevation planes when the MIMO antenna is excited at each port alone. (a) $\phi = 0°$, Port 1. (b) $\phi = 90°$, Port 1. (c) $\phi = 0°$, Port 2. (d) $\phi = 90°$, Port 2. (e) $\phi = 0°$, Port 3. (f) $\phi = 90°$, Port 3. (g) $\phi = 0°$, Port 4. (h)$\phi = 90°$, Port 4.

6. SUMMARY OF THE PROPOSED MIMO ANTENNA PERFORMANCE

This section is concerned with providing a summary of the most important performance metrics for the quad-band patch antenna as well as the MIMO antenna systems proposed in the present work.

6.1. Performance of the Single-Element Antenna

A summary of some important performance measures of the single-element antenna, introduced in Section 2 to construct the proposed MIMO antenna systems at the four operational frequencies, is listed in Table 3.

Table 3. Achieved frequency bands (obtained experimentally) by the proposed quad-band patch antenna and the corresponding gain and radiation efficiency.

Center Frequency (GHz)	Start Frequency (GHz)	End Frequency (GHz)	Bandwidth (GHz)	Gain (dBi)	Radiation Efficiency
28	27.70	28.30	0.60	7.30	86.5%
45	44.50	46.50	2.00	7.03	87.5%
51	50.20	52.00	1.80	7.20	89.2%
56	55.70	57.00	1.30	8.03	90.0%

6.2. Performance of the MIMO Antennas

A comparative performance among some millimetric-wave MIMO antennas designed for mobile handsets that is available in some recent literature, and the MIMO antennas proposed in the present work can be achieved by demonstrating the most important performance as listed in Table 4.

Table 4. Comparison among some millimetric-wave MIMO antennas available in some recent literature and the MIMO antennas proposed in the present work.

Work:		[5]	[11]	[9]	[13]	[14]	Present
Number of ports		7	4	2	2	4	4
Polarization	Co-polarized	√	√	√	√	√	√
	Cross-polarized	×	√	×	√	×	√
Minimum port isolation (dB)		−22	−23	−27	−23	−45	−20
Dimensions (mm^2)		60×25	44×44	55×110	75×40	47×33	20×20
Maximum ECC		0.01	0.0001	NA	0.0001	0.001	0.01
Minimum DG		9.955	9.9999	NA	9.9999	9.995	9.95
Operational frequencies (GHz)	Band 1	37.5	28	28	28	38	28
	Band 2	×	37.5	38	39	×	43
	Band 3	×	×	×	×	×	52
	Band 4	×	×	×	×	×	57
Bandwidth (GHz) at each frequency	Band 1	1.11	1.2	1.1	3.5	3.2	0.60
	Band 2	×	2.0	1.0	4.0	×	0.60
	Band 3	×	×	×	×	×	1.80
	Band 4	×	×	×	×	×	1.50
Gain (dBi) at each frequency	Band 1	7.7	8.0	7.0	5.0	6.5	7.30
	Band 2	×	13.6	8.0	5.7	×	7.03
	Band 3	×	×	×	×	×	7.20
	Band 4	×	×	×	×	×	8.03
Antenna efficiency at each frequency	Band 1	NA	97%	91.2%	99.5%	80%	86.5%
	Band 2	×	98%	89.6%	98.6%	×	87.5%
	Band 3	×	×	×	×	×	89.2%
	Band 4	×	×	×	×	×	90.0%

7. CONCLUSION

Novel designs for compact-size quad-band four-port MIMO antenna systems are introduced for the forthcoming generations of handsets for mobile communications over four frequency bands centered at 28, 43, 52, and 57 GHz. It is shown that the proposed MIMO antennas are well designed to produce appropriate radiation patterns and good impedance matching in the four frequency bands of operation. One of the proposed four-port MIMO antennas provides spatial diversity whereas the other type is cross-polarized and provides both spatial and polarization diversities. The performance of both the quad-band patch antenna and the MIMO antenna systems are assessed including the return loss at each antenna port and the coupling coefficients between the different ports. It is shown that the simulation results agree with the experimental measurements and both show good performance of all the proposed types of MIMO antennas. The bandwidths achieved around 28, 43, 52, and 57 GHz are, respectively, 0.6, 0.6, 1.8, and 1.5 GHz. Also, the radiation efficiencies calculated at the four operational frequencies are 86.5%, 87.5%, 89.2%, and 90.0%, respectively. It is shown that the ECC and the DG are perfect over the four operational frequency bands for all the proposed types of four-port MIMO antenna systems.

REFERENCES

1. Bhatti, R., J. Choi, and S. Park, "Quad-band MIMO antenna array for portable wireless communications terminals," *IEEE Antennas and Wireless Propagation Letters*, Vol. 8, 129–132, 2009.
2. Wong, H. S., S. Kibria, M. T. Islam, J. S. Mandeep, and N. Misran, "Quad band handset antenna for LTE MIMO and WLAN application," *International Journal of Antennas and Propagation*, 2014.
3. Mishra, M. and R. S. Kshetrimayum, "Compact quad-band MIMO antenna array with low mutual coupling for mobile terminal," *IEEE Region 10 Symposium (TENSYMP)*, 665–670, June 2019.
4. Rajagopal, C., N. Noorullakhan, S. B. Suseela, and R. Sankararajan, "Compact modified circular patch quad-band MIMO antenna with high isolation and low correlation," *International Journal of Microwave and Wireless Technologies*, Vol. 9, No. 3, 581–590, 2017.
5. Şeker, C., T. Ozturk, and M. Güneşer, "A single band antenna design for future millimeter wave wireless communication at 38 GHz," *European Journal of Engineering and Formal Sciences*, Vol. 2, No. 2, 35–39, 2018.
6. Eldesouki, E. M., K. F. A. Hussein, and A. M. El-Nadi, "Circularly polarized arrays of cavity backed slot antennas for X-band satellite communications," *Progress In Electromagnetics Research*, Vol. 9, 179–198, 2008.
7. Hussein, K. F. A., "Conical linear spiral antenna for tracking, telemetry and command of low earth orbit satellites," *Progress In Electromagnetics Research*, Vol. 29, 97–107, 2012.
8. Elkady, O. A., S. A. Abolkassem, A. H. Elsayed, W. A. Hussein, and K. F. A. Hussein, "Microwave absorbing efficiency of Al matrix composite reinforced with nano-Ni/SiC particles," *Results in Physics*, Vol. 12, 687–700, 2019.
9. Marzouk, H., M. I. Ahmed, and A. H. Shaalan, "Novel dual-band 28/38 GHz MIMO antennas for 5G mobile applications," *Progress In Electromagnetics Research C*, Vol. 93, 103–117, 2019.
10. Riaz, M. J., A. Sultan, M. Zahid, A. Javed, Y. Amin, and J. Loo, "MIMO antennas for future 5G communications," *2020 IEEE 23rd International Multitopic Conference (INMIC)*, 1–4, IEEE, 2020.
11. Aghoutane, B., S. Das, M. EL Ghzaoui, B. T. P. Madhav, and H. El Faylali, "A novel dual band high gain 4-port millimeter wave MIMO antenna array for 28/37 GHz 5G applications," *AEU — International Journal of Electronics and Communications*, 154071, 2021.
12. Katragadda, S. and P. V. Y. Jayasree, "MIMO antenna miniaturization standards for future 5G," *International Journal of Intelligent Unmanned Systems*, March 2, 2021.
13. Ali, W., S. Das, H. Medkour, and S. Lakrit, "Planar dual-band 27/39 GHz millimeter-wave MIMO antenna for 5G applications," *Microsystem Technologies*, Vol. 27, No. 1, 283–292, 2021.
14. Sehrai, D. A., M. Asif, N. Shoaib, M. Ibrar, S. Jan, M. Alibakhshikenari, A. Lalbakhsh, and E. Limiti, "Compact quad-element high-isolation wideband MIMO antenna for mm-wave applications," *Electronics*, Vol. 10, No. 11, 1300, 2021.
15. El-Hassan, M. A., A. E. Farahat, and K. F. A. Hussein, "Compact-size quad-band patch and MIMO antenna system for 5G mobile handsets," *Progress In Electromagnetics Research C*, Vol. 112, 221–238, 2021.
16. El-Hassan, M. A., A. E. Farahat, and K. F. A. Hussein, "Quad-band MIMO antenna system for 5G mobile handsets," *The Applied Computational Electromagnetics Society Journal (ACES)*, Vol. 36, No. 11, 2021.
17. Farahat, A. E. and K. F. A. Hussein, "Dual-band (28/38 GHz) MIMO antenna system for 5G mobile communications with efficient DoA estimation algorithm in noisy channels," *The Applied Computational Electromagnetics Society Journal (ACES)*, Vol. 36, No. 3, 282–294, 2021.
18. Farahat, A. E. and K. F. A. Hussein, "28/38 GHz dual-band Yagi-Uda antenna with corrugated radiator and enhanced reflectors for 5G MIMO antenna systems," *Progress In Electromagnetics Research C*, Vol. 101, 159–172, 2020.

19. Farahat, A. E. and K. F. A. Hussein, "Dual-band (28/38 GHz) Yagi-Uda antenna with corrugated radiator and triangular reflectors for 5G mobile phones," *The Applied Computational Electromagnetics Society Journal (ACES)*, Vol. 36, No. 10, 1325–1334, 2021.
20. Recioui, A. and H. Bentarzi, "Genetic algorithm based MIMO capacity enhancement in spatially correlated channels including mutual coupling," *Wireless Personal communications*, Vol. 63, No. 3, 689–701, 2012.
21. Recioui, A., "Capacity optimization of MIMO systems involving conformal antenna arrays using a search group algorithm," *Algerian Journal of Signals and Systems*, Vol. 5, No. 4, 209–214, 2020.